ACS APPLIED MATERIALS & INTERFACES

Research Article

www.acsami.org

Pyrene and Diketopyrrolopyrrole-Based Oligomers Synthesized via Direct Arylation for OSC Applications

Shi-Yong Liu,[†,‡] Wen-Qing Liu,[†] Jing-Qi Xu,[†] Cong-Cheng Fan,[†] Wei-Fei Fu,[†] Jun Ling,[†] Jun-Yong Wu,[‡] Min-Min Shi,[†] Alex K.-Y. Jen,*[,†,§] and Hong-Zheng Chen*[,†]

[†]MOE Key Laboratory of Macromolecular Synthesis and Functionalization, State Key Laboratory of Silicon Materials, and Department of Polymer Science and Engineering, Zhejiang University, Hangzhou 310027, P. R. China

[‡]Department of Pharmacy & Chemistry, Taizhou University, Taizhou 317000, P. R. China

[§]Department of Materials Science and Engineering, University of Washington, Seattle, Washington 98198, United States

Supporting Information

ABSTRACT: In this report, an atom efficient and facile synthetic strategy for accessing multi-diketopyrrolopyrrole (DPP)-based oligomers used in solution-processed organic field effect transistors (OFETs) and organic solar cells (OSCs) has been developed. The DPP units were successfully installed onto benzene and pyrene cores via palladium-catalyzed dehydrohalogenative coupling of mono-capped DPPs with multi-bromo-benzene or -pyrene (direct arylation), affording four oligomer small molecules (**SMs 1−4**) containing bis-, tri-, tri-, and tetra-DPP, respectively, in high yields of 78−96%. All the designed linear or branched DPP-based oligomers exhibit broad light absorptions, narrow band-gaps (1.60−1.73 eV), deep highest occupied molecular orbital (HOMO) levels (−5.26 ∼ −5.18 eV), and good thermal stability (Td = 390−401 °C). OFETs based on **SMs 1−4** showed hole mobilities of 0.0033, 0.0056, 0.0005, and 0.0026 $cm^2 V^{-1} s^{-1}$, respectively. OSCs based on **SMs 1−4** under one sun achieved power conversion efficiencies of 3.00%, 3.71%, 2.47%, and 1.86% accordingly, along with high open-circuit voltages of 0.86−0.94 V. For OSC devices of **SM 1**, **SM 3**, and **SM 4**, the solvent $CHCl_3$ was solely employed to the formation of active layers; neither high boiling point additives nor annealing post-treatment was needed. Such a simple process benefits the large-scale production of OSCs via roll to roll technology.

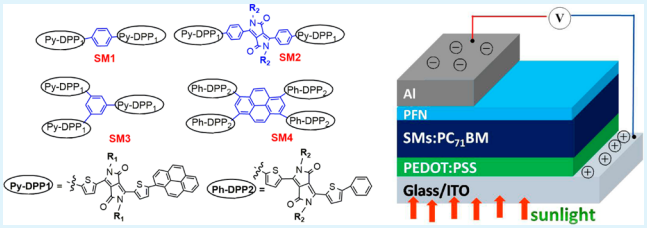

KEYWORDS: *solution-processed small molecules, diketopyrrolopyrrole, pyrene, direct arylation, organic field effect transistors, organic solar cells*

1. INTRODUCTION

In recent years, oligomers and small molecule organic semiconductors for organic solar cells (OSCs) have received great attention, because of their merits of well-defined molecular structure, definite molecular weight, high mobility and open circuit voltage, and high purity with little batch to batch variations.[1−6] Diketopyrrolopyrrole (DPP) chromophore has been extensively explored for organic optoelectronic applications due to its unique π-conjugated system, high optical density, and exceptional stability.[7−10] DPP-based oligomers or small molecules (SM) are widely used for OSCs,[11−31] organic field effect transistors (OFETs),[32−35] dye-sensitized solar cells,[36−38] chemical sensors,[39−41] etc. Besides linear DPP derivatives, DPP-based branched oligomers used for OSCs have also been intensively studied very recently.[3,15,20,24,42] DPP derivatives are usually synthesized via Suzuki, Stille, or Negishi cross-coupling reactions.[11−29,43] Nevertheless, palladium-catalyzed dehydrohalogenative coupling of heteroarenes with aryl halides (known as direct arylation, DA), which does not need organometallic reactants, has emerged as an atomically efficient and viable alternative to these classical cross-coupling reactions.[44−52] Taking into account the cost of materials that are used for devices, developing atom efficient, green, and cost-effective synthetic approaches to π-conjugated (macro) molecules will be highly desirable for the large-scale production of these materials for optoelectronic applications.[46,53,54] Very recently, our group and others have demonstrated that the α-C−H bonds of thiophene−DPPs can be directly arylated by aryl bromides under palladium catalysis, leading to various DPP derivatives.[55−57] Inspired by our previous results,[55,58] we developed herein an effective strategy for the synthesis of structurally complicated multi-DPPs based on the DA reaction of multi-bromo-arenes with mono-capped DPPs. It is worthwhile to explore the new strategy for accessing multi-DPP based oligomers, because multi-DPPs are suggested to perform better than mono-DPPs and bis-DPPs, for OSCs.[22]

Polycyclic aromatic pyrene has acted herein as a partner to integrate with DPP. Pyrene is one of the most frequently

Received: January 24, 2014
Accepted: April 10, 2014
Published: April 10, 2014

   dx.doi.org/10.1021/am500522x | ACS Appl. Mater. Interfaces 2014, 6, 6765−6775

applied building blocks in fluorescence labeled materials.[59,60] Pyrene-based derivatives have also been used as active components in electronic devices such as organic light emitting diodes,[61−68]OFETs,[69] and, more recently, OSCs.[70,71] Structurally, there are 10 positions surrounding the rings of pyrene, which can be potentially bonded to functional groups, leading to multi-functionalized pyrenes. Conventionally, multiaryl functionalized pyrenes are synthesized via Suzuki or Stille cross-coupling of arylboronic acids or aryl-stannanes with multi-bromo-pyrene.[61−67,69−71] To the best of our knowledge, there have been no examples of the application of DA reaction to multi-functionalized pyrene synthesis, although it would be a powerful method for the construction of the pyrene-based materials. In this study, chromophoric DPP and fused aromatic pyrene have been bonded together via DA reaction. And all the synthesized oligomers exhibit broad absorption bands from the visible to near-infrared region, as well as appropriate frontier energy levels, which are suitable for OSC applications. The weak donating power and good planarity of the incorporated pyrene were expected to enhance both open-circuit voltage (V_{OC}) and short-circuit current (J_{SC}) for OSCs, due to its deepened HOMO level[71] and effective $\pi-\pi$ stacking.[21] With these advantages in mind, the solution-processed OFETs and the bulk heterojunction (BHJ) OSC devices based on our DPP−pyrene-based molecules have been fully investigated. It is noteworthy that the previous studies on DA reactions for π-conjugated functional materials were mainly focused on the synthetic methodology; the electronic device performances of the functional materials derived from DA reaction have rarely been reported.[58]

2. EXPERIMENTAL DETAILS

2.1. Instruments and Materials. All ^{1}H and ^{13}C NMR spectra were obtained in chloroform-*d*, unless otherwise noted, with Aglient 600, Bruker DMX-500, or Bruker DMX-300. ^{13}C NMR (126 or 76 MHz) spectra were measured with a proton-decoupling pulse program. Chemical shifts for ^{1}H and ^{13}C NMR were referenced to residual signals from $CDCl_3$ (^{1}H NMR δ = 7.26 ppm and ^{13}C NMR δ = 77.23 ppm). Matrix-assisted laser desorption/ionizationtime of flight mass spectrometry (MALDI-TOF MS) was performed on a Voyager DE STR using 2,5-dihydroxybenzoicacid or α-cyano-4-hydroxycinnamicacid as the matrixes. Samples were prepared by diluting the molecules in chloroform with the matrix. Elemental analyses were conducted on a Flash EA 1112 elemental analyzer. Thermogravimetric analysis (TGA) curves and differential scanning calorimetry (DSC) were measured on a WCT-2 thermal balance. UV−vis spectra were taken on a Shimadzu UV-2450 spectrophotometer. Cyclic voltammetry (CV) was done on a CHI 660C electrochemical workstation with Pt disk, Pt plate, and standard 10 calomel electrode (SCE) as working electrode, counter electrode, and reference electrode, respectively, in a 0.1 mol L^{-1} tetrabutylammonium hexafluorophosphate (Bu_4NPF_6) CH_2Cl_2 solution. Theoretical calculations based on density functional methods have been performed for compounds **SMs 1−4** with the Gaussian09 program.[72] Becke's three-parameter[73] gradient-corrected functional (B3LYP) with 6-31G(d,p) basis was used to optimize the geometry and to compute the electronic structure at the minima found. The determination of the dihedral angle was achieved using Gaussview. The X-ray diffraction (XRD) measurement with an out-of-plane arrangement was performed on a RIGAKU D/MAX 2550/PC rotating anode X-ray diffract meter equipped with a Cu Kα tube and Ni filter (λ = 0.1542 nm). The current-voltage ($J-V$) curves were measured with Keithley 2400 measurement source units at room temperature in air. The photocurrent was measured under a calibrated solar simulator (Abet 300 W) at 100 mW cm^{-2}. Topographic images of the films were obtained on a Veeco MultiMode atomic force microscopy (AFM) in the tapping mode.

All starting organic compounds were purchased from Aldrich, Alfa Aesar, Alladin, Energy chemical, or TCI and used without further purification. The reaction medium dimethylacetamide (DMA) was anhydrous.

2.2. Fabrication of OFETs and OSC Devices. For OFETs, a heavily doped silicon wafer was used as the gate electrode and substrate, with a 300 nm thermally oxidized SiO_2 layer as a gate insulator modified with divinyltetramethyldisiloxane bis(benzocyclobutene) (BCB). The **SMs 1−4** films were cast from chloroform solution. FETs were constructed in a bottom-gated configuration by depositing top-contact source and drain electrodes (70 nm Au), with a channel length of 50 μm and width of 1 mm. Current−voltage characteristics of the devices were measured in air using a Keithley 4200-SCS semiconductor parameter analyzer. The measured capacitance of the BCB-covered SiO_2/Si substrates was 10 nF cm^{-2}, and this value was used for mobility calculation.

Solar cells were fabricated on glass substrates commercially pre-coated with a layer of indium tin oxide (ITO). The substrates were prior cleaned using detergent, deionized water, acetone, and isopropanol consecutively for every 15 min and then treated in an ultraviolet ozone generator for 15 min before being spin-coated with a layer of 35 nm poly(3,4-ethylenedioxythiophene):poly(styrenesulfonate) (PEDOT:PSS). After baking the PEDOT:PSS in air at 140 °C for 15 min, the substrates were transferred to a glove box. The BHJ layer was spin-cast from a solution of small molecules and $PC_{61}BM$ in chloroform at a total solid concentration of 16 mg mL^{-1}. The thickness of the active layer was tuned by adjusting the concentration of the solutions and the spin-coating speed. The poly[(9,9-bis(3′-(*N*,*N*-dimethylamino)propyl)-2,7-fluorene)-*alt*-2,7-(9,9-dioctylfluorene)] (PFN) interlayer material was dissolved in methanol, and its solution (concentration, 2 mg mL^{-1}) was spin-coated on top of the active layers. Then the samples were loaded into a vacuum deposition chamber (background pressure $\approx 5 \times 10^{-4}$ Pa) to deposit 120 nm thick aluminum cathode with a shadow mask (device area of 4 mm^2).

The current−voltage ($I-V$) curves were measured with Keithley 2400 measurement source units at room temperature in air. The photocurrent was measured under a calibrated solar simulator (Abet 300 W) at 100 mW cm^{-2}, and the light intensity was calibrated with a standard silicon photovoltaic reference cell.

2.3. Synthetic Procedures. The general synthetic routes toward **SMs 1−4** are outlined in Scheme 1. The detailed synthetic procedures are as follows.

*1. $Py_2PhTh_4(DPP)_2$ (**SM 1**).* **Py-DPP1** (330 mg, 0.35 mmol), 1,4-dibromobenzene (37.2 mg, 0.16 mmol), anhydrous K_2CO_3 (54.5 mg, 0.40 mmol), PivOH (4.8 mg, 0.11 mmol), and $Pd(OAc)_2$ (3.5 mg, 0.017 mmol) were stirred in anhydrous DMA (5 mL) at 110 °C for 10 h under nitrogen atmosphere in a Schlenk tube. After cooling to room temperature, the mixture was poured into a 150 mL aqueous solution of NaCl to remove the salts and high boiling point solvent DMA. The precipitate was extracted with CH_2Cl_2 (3 × 20 mL). The combined

Scheme 1. Synthetic Routes of SMs 1−4

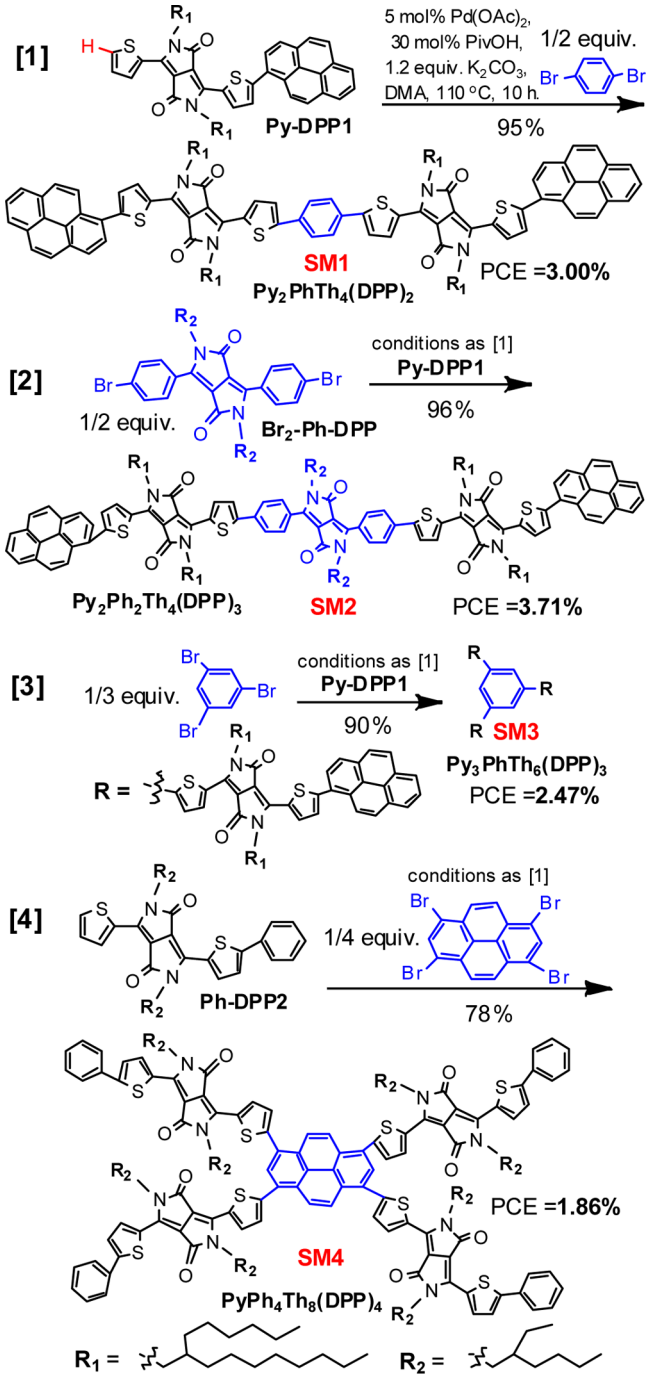

organic layer was washed with distilled water. Removal of the CH_2Cl_2 by rotary evaporator afforded the crude product, which was then purified by column chromatography on silica gel using the mixtures of CH_2Cl_2 and petroleum ether as eluent (2:1, v/v) and gave a dark blue solid, **SM 1** (290 mg, yield 95%).

^{1}H NMR (600 MHz, $CDCl_3$) δ 9.07 (d, J = 95.8 Hz, 4H), 8.52 (d, J = 9.0 Hz, 2H), 8.12 (dd, J = 78.9, 25.5 Hz, 16H), 7.80−7.31 (m, 8H), 4.08 (s, 8H), 2.04 (d, J = 34.3 Hz, 4H), 1.38 (s, 25H), 1.33−1.13 (m, 77H), 0.83 (dd, J = 31.1, 6.9 Hz, 25H).

^{13}C NMR (151 MHz, $CDCl_3$) δ 161.75, 148.48, 140.06, 139.57, 136.54, 133.38, 131.68, 131.47, 130.90, 130.42, 129.46, 128.96, 128.72, 128.14, 128.13, 128.12, 127.29, 126.47, 125.66, 125.42, 125.26, 125.15, 124.73, 124.48, 108.19, 32.01, 31.47, 30.24, 29.97, 29.67, 29.45, 26.49, 26.45, 22.77, 14.25.

MALDI-TOF MS (m/z): $[M]^+$ calcd for $C_{130}H_{162}N_4O_4S_4$, 1972.69; found, 1972.10. Elemental anal. calcd: C, 79.14; H, 8.28; N, 2.84. Found: C, 79.01; H, 8.31; N, 2.82.

*2. $Py_2Ph_2Th_4(DPP)_3$ (**SM 2**).* **Py-DPP1** (800 mg, 0.84 mmol), **Br_2-Ph-DPP** (250 mg, 0.37 mmol), anhydrous K_2CO_3 (130 mg, 0.93 mmol), PivOH (22.8 mg, 0.25 mmol), and $Pd(OAc)_2$ (8.4 mg, 0.04 mmol) were stirred in anhydrous DMA (5 mL) at 110 °C for 10 h under nitrogen atmosphere in a Schlenk tube. The post-treatment of the reactions are similar to those of **SM 1**. The crude product was purified by column chromatography on silica gel using the mixtures of CH_2Cl_2 and petroleum ether as eluent (5:1, v/v) and gave a dark blue solid, **SM 2** (850 mg, yield 96%).

^{1}H NMR (600 MHz, $CDCl_3$) δ 9.18 (d, J = 90.6 Hz, 4H), 8.15 (s, 2H), 7.87 (s, 2H), 7.77-7.16 (dd, J = 210.0 Hz, 26H), 4.41- 3.19 (d, J = 93.7 Hz, 12H), 1.99 (d, J = 78.8 Hz, 6H), 1.34−0.72 (t, J = 187.3 Hz, 148H).

Due to the aggregation of **SM 2** in $CDCl_3$, the sample in solution was below the ^{13}C NMR detection limit. ^{13}C NMR signals, especially for aromatic areas, could not be observed (Supporting Information Figure S7).

MALDI-TOF MS (m/z): $[M]^+$ calcd. for $C_{158}H_{200}N_6O_6S_4$, 2407.58; found, 2408.61. Elemental Anal. calcd: C, 78.82; H, 8.37; N, 3.49. Found: C, 78.63; H, 8.40; N, 3.45.

*(3). $Py_3PhTh_6(DPP)_3$ (**SM 3**).* **Py-DPP1** (330 mg, 0.35 mmol), 1,4-dibromobenzene (33.2 mg, 0.12 mmol), anhydrous K_2CO_3 (54.5 mg, 0.40 mmol), PivOH (4.8 mg, 0.11 mmol), and $Pd(OAc)_2$ (3.5 mg, 0.017 mmol) were stirred in anhydrous DMA (10 mL) at 110 °C for 10 h under nitrogen atmosphere in a Schlenk tube. The post-treatments of the reaction are similar to those of **SM 1**. The crude product was purified by column chromatography on silica gel using the mixtures of CH_2Cl_2 and petroleum ether as eluent (3:1, v/v) and gave a blue purple solid, **SM 3** (320 mg, yield 90%).

^{1}H NMR (600 MHz, $CDCl_3$) δ 9.13 (s, 3H), 8.91 (s, 3H), 8.44 (s, 3H), 7.93 (ddd, J = 103.1, 73.2, 30.1 Hz, 27H), 7.50 (d, J = 20.4 Hz, 6H), 4.06 (s, 12H), 2.00 (d, J = 40.3 Hz, 6H), 1.22 (dd, J = 79.3, 42.2 Hz, 154H), 0.74 (d, J = 5.8 Hz, 38H).

^{13}C NMR (151 MHz, $CDCl_3$) δ 164.27, 149.76, 143.19, 141.72, 139.29, 137.78, 134.18, 133.97, 133.39, 132.93, 132.75, 131.96, 131.44, 131.25, 131.02, 130.88, 130.75, 130.68, 129.77, 129.00, 128.51, 128.21, 127.49, 127.22, 126.95, 111.41, 49.07, 40.62, 40.50, 34.53, 34.05, 32.79, 32.45, 32.26, 32.00, 29.05, 25.33, 16.76.

MALDI-TOF MS (m/z): $[M]^+$ calcd for $C_{192}H_{240}N_6O_6S_6$, 2925.39; found, 2925.71. Elemental Anal. calcd: C, 78.96; H, 8.28; N, 2.88. Found: C, 78.35; H, 8.30; N, 2.86.

*(4). $PyPh_4Th_8(DPP)_4$ (**SM 4**).* **Ph-DPP2** (440 mg, 0.74 mmol), 1,3,6,8-tetrabromopyrene (77 mg, 0.15 mmol), anhydrous K_2CO_3 (100 mg, 0.74 mmol), PivOH (18.2 mg, 0.18 mmol), and $Pd(OAc)_2$ (6.2 mg, 0.03 mmol) were stirred in anhydrous DMA (8 mL) at 110 °C for 10 h under nitrogen atmosphere in a Schlenk tube. The post-treatments of the reaction are similar to those of **SM 1**. The crude product was purified by column chromatography on silica gel using the mixtures of CH_2Cl_2 and petroleum ether as eluent (5:1, v/v) and gave a dark blue solid, **SM 4** (301 mg, yield 78%).

^{1}H NMR (500 MHz, $CDCl_3$) δ 9.07 (d, J = 46.8 Hz, 8H), 8.57 (s, 4H), 8.32 (s, 2H), 7.80-7.51 (m, 12H), 7.38 (d, d, J = 38.7 Hz, 16H), 4.12 (s, 16H), 2.00 (s, 8H), 1.39-1.14 (m, 64H), 0.94−0.78 (m, 48H).

dx.doi.org/10.1021/am500522x | ACS Appl. Mater. Interfaces 2014, 6, 6765−6775

Due to the aggregation of **SM 4** in $CDCl_3$, the sample in solution was below the ^{13}C NMR detection limit. ^{13}C NMR signals, especially for aromatic area, could not be observed (Supporting Information Figure S9).

MALDI-TOF MS (*m/z*): $[M]^+$ calcd for $C_{160}H_{178}N_8O_8S_8$, 2597.69; found, 2598.03. Elemental Anal. calcd: C, 73.98; H, 6.91; N, 4.30. Found: C, 73.55; H, 7.00; N, 4.27.

3. RESULTS AND DISCUSSION

3.1. Synthesis. Scheme 1 shows the synthetic routes of the four pyrene−DPP-based oligomers. The parent mono-pyrenyl and mono-phenyl terminated DPPs, **Py-DPP1** and **Ph-DPP2**, were synthesized by Suzuki couplings of mono-bromo−DPPs with pyren-1-ylboronic acid and phenylboronic acid, respectively. To ensure enough solubility of the final oligomers in common solvents, alkyl groups 2-hexyl-decyl ($\mathbf{R_1}$) or 2-ethyl-hexyl ($\mathbf{R_2}$) were pre-installed on the nitrogen atoms of the starting DPPs (for detailed procedures and synthetic routes for the parent DPPs, see Supporting Information, Schemes S1 and S2). Since one of the thiophene rings of **Py-DPP1** or **Ph-DPP2** is end-capped by pyrenyl or phenyl groups, the arylation of the single remaining α-C−H bond on the other side by multi-bromo-arenes will lead to formation of multi-DPP-substituted arenes. This strategy should make the multi-DPPs facilely accessible, because of the high reactivity of the thiophene α-C−H bonds in DPPs for DA reactions.[55−57]As shown by reaction [1] in Scheme 1, the DA reaction of **Py-DPP1** with *p*-dibromobenzene under simple and ligandless conditions, 5 mol % $Pd(OAc)_2$, 30 mol % pivalic acid (PivOH), 1.2 equiv K_2CO_3, and anhydrous dimethylacetamide (DMA) at 110 °C for 10 h, gave the target bis-DPP in 95% yield. The resulting linear oligomer has two DPP units, two pyrenyl (**Py**) groups, four thiophene (**Th**) rings, and one benzene (**Ph**) core and thus was named as $\mathbf{Py_2PhTh_4(DPP)_2}$ (**SM 1**) accordingly. Furthermore, the DA coupling of **Py-DPP1** with *p*-bromobenzene-connected DPP ($\mathbf{Br_2}$**-Ph-DPP**) under the same conditions gave a linear tri-DPP, $\mathbf{Py_2Ph_2Th_4(DPP)_3}$ (**SM 2**), with an excellent yield of 96%. Using similar conditions, the arylation of **Py-DPP1** and **Ph-DPP2** by 1,3,5-tribromobenzene and 1,3,6,8-tetrabromo-pyrene afforded tri- and tetra-DPP dendrimers, phenyl-centred $\mathbf{Py_3PhTh_6(DPP)_3}$ (**SM 3**) and pyrene-centred $\mathbf{PyPh_4Th_8(DPP)_4}$ (**SM 4**), in yields of 90% and 78%, respectively (reactions [3] and [4] in Scheme 1). As discussed above, the bis-, tri-, and tetra-DPP units have been successfully installed onto benzene and pyrene centres by DA reaction just in one step, leading to **SMs 1−4**. In these reactions, the use of organometallic reactants was avoided. Remarkably, even though the reactant 1,3,6,8-tetrabromopyrene has no observable solubility in reaction medium DMA, during the reaction it can be consumed completely and converted effectively to the product **SM 4**. This observation suggests that the α-C−H bonds of Th-DPPs are highly reactive toward DA reaction under present catalysis, keeping the reaction equilibrium shifting to the right even for the little soluble aryl bromide reactants.

3.2. Characterizations and Optical Properties. To ensure a high purity for high performances, all **SMs** have been purified two times by column chromatography followed by re-crystallization in CH_2Cl_2−CH_3OH mixed solvent before being employed to characterizations and device fabrication. These molecules have been well characterized by ^1H and ^{13}C NMR, MALDI-TOF MS, elemental analysis, thermogravimetric analysis (TGA), and XRD. Figure 1 shows the TGA curves of **SMs**. **SMs 1−4** all exhibit good thermal stability, with 5% weight-loss temperatures (T_d) at 390, 408, 399, and 401 °C under N_2 protection, respectively.

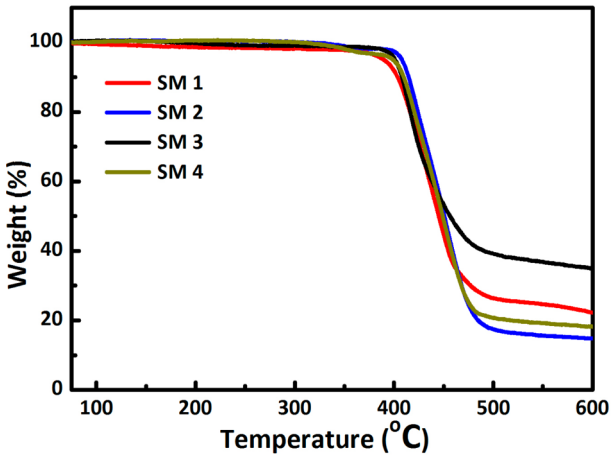

Figure 1. TGA curves of **SMs 1−4**.

UV−vis absorption spectra and cyclic voltammetry (CV) were applied to study the optical and electrochemical properties of **SMs 1−4**. Figure 2 shows the UV−vis spectra of the four oligomers in $CHCl_3$ solution and as thin solid films. All **SMs** exhibit broad absorption bands in the visible to near-infrared region. The significant optical properties are listed in Table 1. The absorption peaks of **SMs 1−4** in $CHCl_3$ solution (λ_{max}^{s}) are 629.0, 624.5, 605.5, and 598 nm, respectively, and the solid films absorption peaks (λ_{max}^{f}) shift to longer wavelengths 640.1, 671.1, 655.8, and 620.5 nm correspondingly, indicating $\pi-\pi$ stacking of the oligomers in solid state was more favorable than in solutions. All spectra of thin film absorptions exhibit strong vibronic shoulder peaks. The absorption band-edges of the cast films (λ_{edge}^{f}) for **SMs 1−4** shift to 761.4, 775.2, 715.2, and 751.1 nm respectively, which correspond to the optical bandgaps (E_g^{opt}) of 1.63, 1.60, 1.73, and 1.65 eV. **SM 2** has the lowest bandgap, because of the enhanced intra-molecular charge transfer from both flank pyrene−thiophene−DPPs to the central benzene−DPP.

3.3. Electrochemical Properties. The redox behavior of the oligomers was investigated by CV in 0.1 M solution of $TBAPF_6$/dichloromethane. The CVs were recorded versus the potential of the SCE, which was calibrated by the ferrocene−ferrocenium (Fc/Fc^+) redox couple. CV curves of **SMs 1−4** are shown in Figure 3, and the electrochemical data are summarized in Table 1. The HOMO energy levels were calculated from the CV, and the corresponding lowest unoccupied molecular orbital (LUMO) levels were estimated from LUMO = HOMO + E_g^{opt}. All oligomers have deep HOMO levels with an average value of ca. −5.20 eV. The pyrene-centered DPP **SM 4** owns the deepest HOMO level (−5.26 eV), due to the butterfly-like twisted structure of the backbone of the multi-aryl-substituted pyrene.[68−70]

To gain a better understanding of the structure−property relationships, the molecular geometries and electron density distribution were simulated using density functional theory (DFT) (Figure 4 and Figures S10−S13, Supporting Information). As shown in Figures 4a,b, the optimized geometries of **SMs 1** and **2** have a linear and planar structure. In contrast, due to the large torsion angles between thiophene rings and

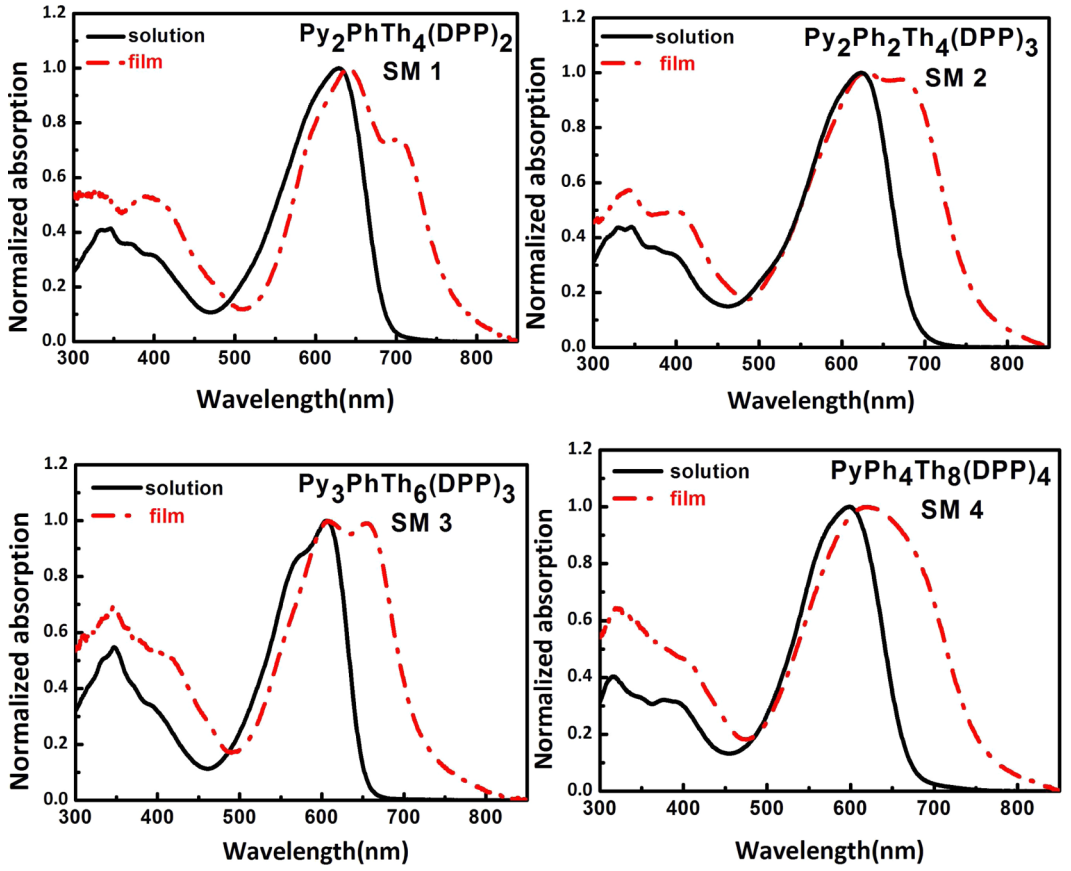

Figure 2. Normalized UV−vis absorption spectra of **SMs 1−4** in $CHCl_3$ and thin films on quartz substrates.

Table 1. Optical and Electrochemical Properties of SMs 1−4

SMs	λ_{max}^{s} (nm)	λ_{max}^{f} (nm)	λ_{edge}^{f} (nm)	E_g^{opt} (eV)	$HOMO^{cv}$ (eV)	E_g^{cal} (eV)	$HOMO^{cal}$ (eV)
SM1	629.0	640.1	761.4	1.63	−5.18	2.46	−5.04
SM2	624.5	671.1	775.2	1.60	−5.19	2.38	−5.07
SM3	605.5	655.8	715.2	1.73	−5.22	2.67	−5.17
SM4	598.0	620.5	751.1	1.65	−5.26	2.53	−5.18

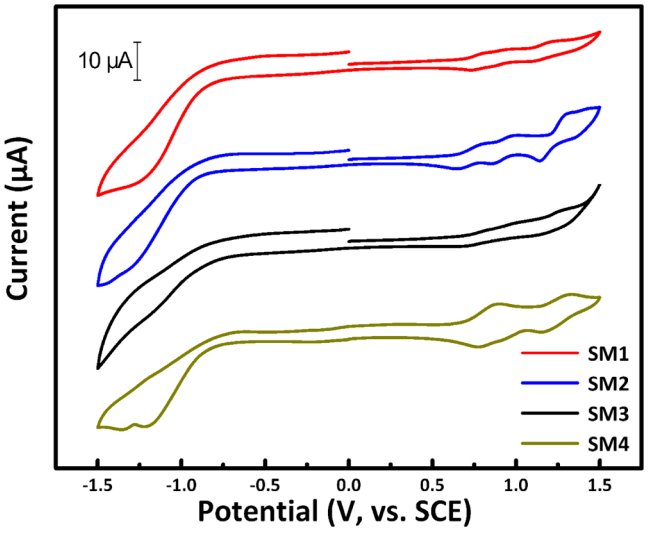

Figure 3. Cyclic voltammograms of **SMs 1−4**.

benzene or pyrene centers, **SMs 3** and **4** possess a twisted and multi-dimensional structure. Similar to the reported multi-aryl substituted pyrenes,[61−63,69] **SM 4** shows a butterfly-like shape (Figure 4d). The DFT-calculated frontier energy levels are listed in Table 1. Generally, for **SMs 1−4**, the electron density in the HOMO is delocalized on the electron donating thiophene and pyrene units; LUMO wave functions are localized on the electron-withdrawing DPPs. Although the theoretically calculated HOMO−LUMO gaps (E_g^{cal}) are higher than those optically obtained (E_g^{opt}) by ca. 0.9 eV, the results from DFT calculation are correlated well with the results from experimental measurement. The **SM 2** has still the lowest calculated band-gap (E_g^{cal}) and **SM 4** has the lowest calculated $HOMO^{cal}$ among the four molecules.

3.4. Molecular Stacking. To further investigate the crystallinities and molecular orientations of the thin films of the **SMs**, X-ray diffraction (XRD) analyses were performed, because the interconnectivity of organic semiconductors, which mainly arises from $\pi-\pi$ interactions, plays a key role in charge transport between adjacent (macro)molecules. Thin films of **SMs 1−4** were drop cast from $CHCl_3$ solutions onto ITO substrates. To gain the information about the effects of annealing treatment on the crystallinities of **SMs**, both the as-cast and the annealed thin films of **SMs** were subjected to XRD measurement. The annealing temperatures are dependent on

dx.doi.org/10.1021/am500522x | ACS Appl. Mater. Interfaces 2014, 6, 6765−6775

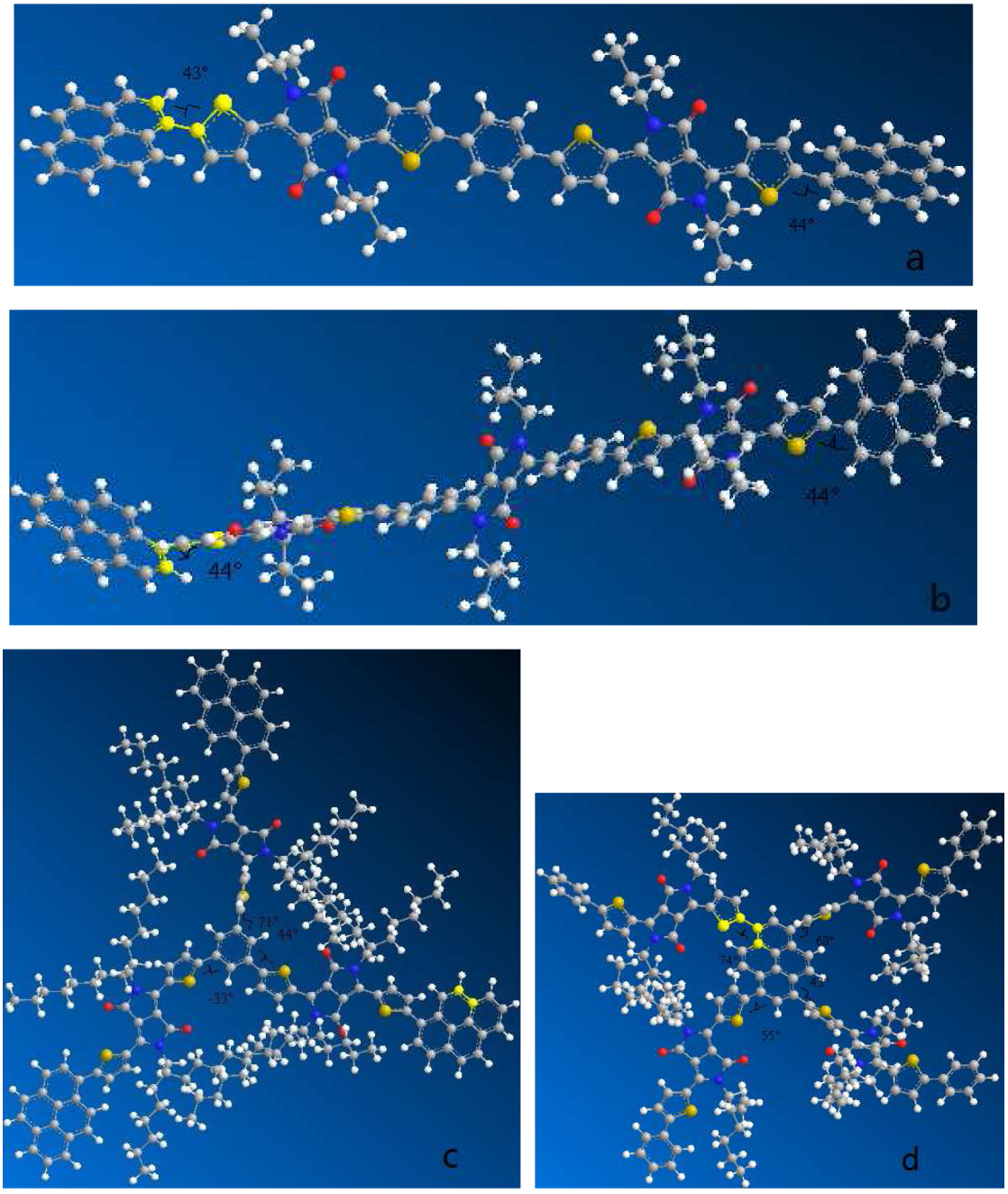

Figure 4. Optimized geometries obtained by DFT calculations (a) **SM1**, (b) **SM 2**, (c) **SM 3**, and (d) **SM 4**.

the crystallization temperatures determined by DSC (Supporting Information Figures S14–S17), that is, 140, 120, 100, and 180°C for **SMs 1–4**, respectively. Figure 5 shows the XRD patterns of these films from **SMs 1–4**.

Among the as-cast films of all **SMs**, **SM 1** and **SM 2** exhibit distinct diffraction peaks in the small angle region, with *d*-spacings of 1.87 and 1.43 nm, respectively. Compared with **SM 1**, **SM 2** owns a sharper diffraction peak in the small angle region. This can be ascribed to the presence of a DPP unit at the center of **SM 2**, leading to stronger intermolecular interactions than **SM 1** and, thus, a longer-range-ordered crystalline structure for **SM 2**. Furthermore, despite that the alkyl chains (16C) of **SM 2** are more steric than those of previously reported tri-DPPs (8C), **SM 2** has a shorter *d*-spacing (1.43 nm) than the reported tri-DPPs (*d*-spacing = 1.53 nm) having no end-groups on the flank thiophene rings.[22] Such a difference indicates that the introduction of pyrene as end-groups effectively enhances intermolecular interactions. As a result, the molecules can be stacked more tightly, leading to a relatively narrower *d*-spacing. This observation will offer a useful reference for the design of pyrene-containing functional (macro)molecules. The promotion of molecular assembly by pyrene end-group has also been evidenced in a previous report.[21] As shown in Figure 5, the annealing treatment led to an increased sharpness for the diffraction peak of **SM 1**, and an additional diffraction peak (*d*-spacing = 1.82 nm) for **SM 2**, indicating the crystallinities of **SM 1** and **SM 2** were improved after annealing treatment. In contrast to **SM 1** and **SM 2**, no clear diffraction peaks among 2θ of 3–20° were observed for the as-cast films of **SM 3** and **SM 4**. It was found that the

dx.doi.org/10.1021/am500522x | ACS Appl. Mater. Interfaces 2014, 6, 6765–6775

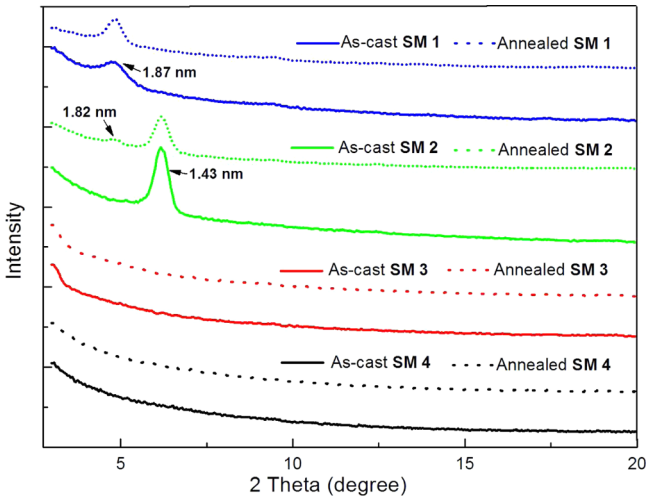

Figure 5. XRD patterns of as-cast and annealed thin films of **SMs 1**–**4**.

annealing treatment has no observable effects on the crystallinities of **SM 3** and **4** (Figure 5). The twisted structures of **SM 3** and **SM 4**, as predicated by DFT calculations, might hinder the lamella stacking among molecules.

The results of XRD analysis for **SMs 1**–**4** were further supported by DSC measurements. As shown in Figures S14–S17 (Supporting Information), all compounds exhibit endothermic peaks during the cooling scan. The enthalpies for **SMs 1**–**4** are found to be 34.74, 21.96, 1.03, and 12.83 J/g, respectively. The enthalpies of **SMs 1** and **2** are higher than those of **SMs 3** and **4**, implying stronger intermolecular interaction and higher crystallinity for the former two, which is in accordance with the XRD findings.

3.5. OFET Performances. Field effect transistors (FETs) were constructed in the bottom-gate and top-contact configuration,with channel length of 50 μm and width of 1 mm. An average charge transport performance of 15 devices for each molecule was summarized in Table 2. For comparison purposes, the OFETs of as-cast and annealed films for each molecule have been independently investigated. The annealing temperatures for **SMs 1**–**4** were 140, 120, 100, and 180 °C, respectively, the same as the crystallization temperature determined by DSC (Supporting Information Figures S14–S17). After thermal annealing, the hole mobilities of **SM 1** and **SM 2** were further enhanced due to their improved crystalinities, while thermal annealing has a negative effect on the mobility of **SM 3** and **SM 4**. The highest hole mobilities of the OFETs based on **SMs 1**–**4** were 0.0033, 0.0056, 0.0005, and 0.0026 $cm^2\ V^{-1}\ s^{-1}$, respectively. **SM 1** and **2** possess higher mobility than **SM 3** and **4**. This can be ascribed to their higher crystalline packing efficiency, as indicated by the XRD curves in Figure 5. Owing to the relatively high hole mobility of **SMs 1**–**4**, efficient charge transport in the solar cells is anticipated.

3.6. OSC Performances. Given the appropriate energy levels, narrow optical bandgaps, broad absorptions, good solubility, good thermal stability, and high hole mobility, the oligomers **SMs 1**–**4** are suitable for use as donors in solution processed BHJ solar cells. For BHJ OSCs, the above DPP–pyrene-based compounds and (6,6)-phenyl-C_{71}-butyric acid methyl ester ($PC_{71}BM$) were used as electronic donors and acceptor, respectively. OSCs of the four small molecules were fabricated by spin-coating **SMs**:$PC_{71}BM$ blends from chloroform onto a clean ITO/PEDOT:PSS bottom electrode on a glass substrate. Optimizations for the donor–acceptor blend ratios, annealing temperatures, and additives were systematically studied. Table 3 and Figure 6 show the power conversion efficiencies (PCEs) of **SMs 1**–**4** under the optimized parameters and the corresponding current density–voltage (J–V) curves. The best PCEs for **SM 1**, **SM 2**, **SM 3**, and **SM 4** were 3.00%, 3.71%, 2.47%, and 1.86%, respectively. For OSC devices of **SM 1**, **3**, and **4**, employments of high boiling point solvent additives and annealing treatments were not necessary (Table 3). Chloroform solvent was solely applied to the active layers formation of these three molecules. Such a simple process benefits the large-scale production of OSCs by roll to roll or printable technology.[21] It is noteworthy that, for **SM 3** and **4**, annealing treatment has also a negative effect on their OFET performances (Table 2). Among the four SMs, **SM 2** has the highest fill factor (FF) and a high V_{OC} (0.91 V), leading to the highest PCE of 3.71%. As discussed, **SM 1** and **2** have higher charge mobility than **SM 3** and **4**. In accordance with this result, **SM 1** and **2** for OSCs also performed better than **SM 3** and **4**. This can be ascribed to their fine planar structures (Figures 4a,b), which would improve the π–π stacking (Figure 5) and increase the charge mobility (Table 2). The dendritic **SM 4** gave a lowest PCE (1.86%) but a highest V_{OC} (0.94 V) due to its lowest HOMO level. The low J_{SC} and FF of **SM 4** could be ascribed to the limited intermolecular π–π stacking as a result of its twisted structure.

It is well known that film morphology plays a key role in the charge separation and charge transfer for the organic thin film solar cells. To investigate the causes for the varied OSC performances of **SMs 1**–**4**, the film morphologies were measured using tapping mode AFM. Figure 7 shows the height and phase images obtained by AFM for **SMs 1**–**4**/$PC_{71}BM$ blended films prepared from their respective optimized conditions listed in Table 3. The **SM 2**/$PC_{71}BM$ blended film is composed of networks with defined crystallites and phase separation with clear boundaries (Figure 7b,f). Compared with the other **SMs**/$PC_{71}BM$ films, **SM 2**/$PC_{71}BM$ film exhibits more distinctive morphology with interconnected domains. These interpenetrating networks of donors and acceptors provide interfaces for exciton dissociations and percolation pathways for charge carrier transport to

Table 2. OFET Performances of the As-Cast and Annealed Films for SMs 1–4[a]

parameters	SM 1	SM 2	SM 3	SM 4
hole mobility ($cm^2\ V^{-1}\ s^{-1}$)	$9.0 \pm 1.2 \times 10^{-5}$ ($2.6 \pm 0.7 \times 10^{-3}$)	$4.0 \pm 1.4 \times 10^{-4}$ ($3.5 \pm 0.8 \times 10^{-3}$)	$3.1 \pm 0.9 \times 10^{-4}$ ($1.2 \pm 0.4 \times 10^{-4}$)	$1.6 \pm 0.4 \times 10^{-3}$ ($4.4 \pm 0.8 \times 10^{-4}$)
I_{on}/I_{off}	$\sim 10^3$ ($\sim 10^3$)	$>10^3$ ($>10^3$)	$>10^3$ ($\sim 10^3$)	$>10^3$ ($\sim 10^3$)
V_T/V	−9.5 ~ −15.1 (−14.0 ~ −22.8)	−16.6 ~ −29.7 (−29.7 ~ −54.3)	−19.6 ~ −42.7 (−20.0 ~ −37.7)	−22.5 ~ −34.4 (−13.0 ~ −18.7)

[a]The values in brackets were obtained from annealed films.

dx.doi.org/10.1021/am500522x | ACS Appl. Mater. Interfaces 2014, 6, 6765–6775

Table 3. Device Performances of the OSCs Based on SMs 1−4

SMs	SMs:$PC_{71}BM$	CN[a](wt %)	T (°C)[b]	V_{OC} (V)	J_{SC}[c]	FF	PCE (%)
SM 1	1:3	w/o	w/o	0.86	9.00	0.39	3.00
SM 2	1.5:1	0.2	120	0.91	8.37	0.49	3.71
SM 3	1:3	w/o	w/o	0.92	7.23	0.37	2.47
SM 4	1:3	w/o	w/o	0.94	5.83	0.34	1.86

[a]1-Chloronaphthalene. [b]Annealing temperatures. [c]As mA cm^{-2}.

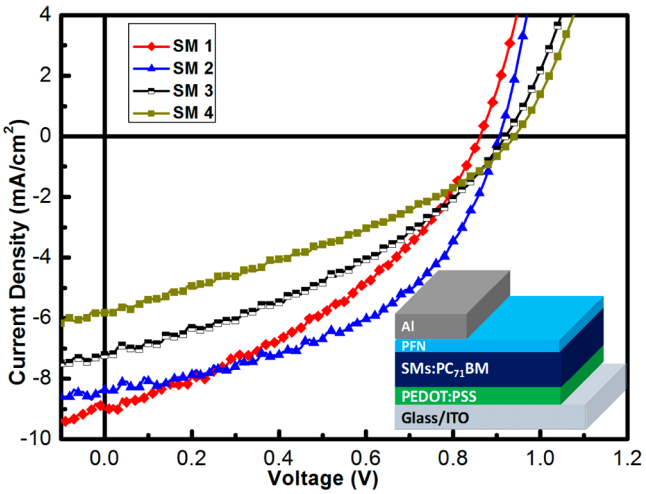

Figure 6. J−V curves of **SMs 1−4** and their device configuration of OSCs (right bottom).

corresponding electrodes, which accounts for the enhanced device performance of **SM 2**. In sharp contrast with **SM 2**, **SM 4**/$PC_{71}BM$ film has an underdeveloped phase separation and unclear boundaries (Figure 7d,h), leading to a relatively poor device performance. These observations indicate that the performances of OSCs are heavily dependent on their film morphology.

4. CONCLUSION

In summary, a series of DPP−pyrene-based new oligomers containing multi-DPP chromophores, which demonstrated fine OFETs and OSC performances, have been designed and facilely accessed by an effective synthetic strategy based on direct arylation of the single α-C−H bond of thiophene−DPPs. The thiophene−DPP can even reacted smoothly with little soluble aryl bromide, 1,3,6,8-tetrabromopyrene, affording the tetra-DPP-functionalized pyrene. The synthesized **SMs 1−4** have been well characterized by ^1H and ^{13}C NMR, MALDI-TOF MS, elemental analysis, TGA-DSC, UV−vis, CV, DFT calculations, XRD, AFM analysis, and OFET and OSC performances. The results indicate that OFET and OSC performances of **SMs 1−4** increase with the increase of planarity of the molecular structures. Our study paves the way for versatile, green, and straightforward synthesis of structurally complicated multi-DPP functional molecules for organic opoto-electronics; the strategy here developed will find applications in a wide range of π-functional units beyond DPPs and pyrenes. The synthesis of multi-DPPs end-capped with aryl groups other than benzene or pyrene, and multi-aryl (other than DPP)-substituted pyrenes via DA reaction and corresponding device performance studies are in progress.

■ ASSOCIATED CONTENT

Ⓢ Supporting Information

The detailed synthetic routes, synthetic procedures, and ^1H NMR spectra of parent DPPs, ^1H and ^{13}C NMR, MALDI-TOF MS spectra, and HOMO and LUMO orbits of **SMs 1−4**. This material is available free of charge via the Internet at http://pubs.acs.org.

■ AUTHOR INFORMATION

Corresponding Authors

*E-mail: hzchen@zju.edu.cn (H.-Z.C.).
*E-mail: ajen@u.washington.edu (A.K.-Y.J.).

Notes

The authors declare no competing financial interest.

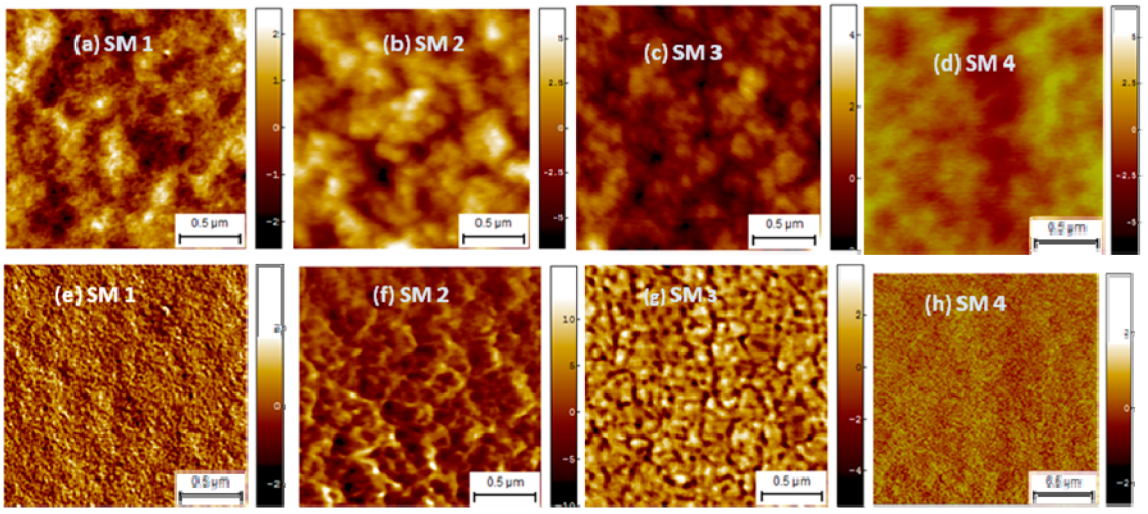

Figure 7. AFM height images (a, b, c, d) and phase images (e, f, g, h) of the **SMs 1−4**/$PC_{71}BM$ blended films prepared from optimized conditions.

■ ACKNOWLEDGMENTS

NSFC (Nos. 21244008, 21374075, 51261130582, and 91233114), 973 Program (No.2014CB643503), FRFCU (2012QNA4025), and 863 Program (No. 2011AA050520) are appreciated for financial support.

■ REFERENCES

(1) Walker, B.; Kim, C.; Nguyen, T.-Q. Small Molecule Solution-Processed Bulk Heterojunction Solar Cells. *Chem. Mater.* **2011**, *23*, 470−482.
(2) Henson, Z. B.; Müllen, K.; Bazan, G. C. Design Strategies for Organic Semiconductors Beyond the Molecular Formula. *Nat. Chem.* **2012**, *4*, 699−704.
(3) Roncali, J. Molecular Bulk Heterojunctions: An Emerging Approach to Organic Solar Cells. *Acc. Chem. Res.* **2009**, *42*, 1719−1730.
(4) Lin, Y.; Li, Y.; Zhan, X. Small Molecule Semiconductors for High-efficiency Organic Photovoltaics. *Chem. Soc. Rev.* **2012**, *41*, 4245−4272.
(5) Chen, Y.; Wan, X.; Long, G. High Performance Photovoltaic Applications Using Solution-Processed Small Molecules. *Acc. Chem. Res.* **2013**, *46*, 2645−2655.
(6) Zhou, J.; Zuo, Y.; Wan, X.; Long, G.; Zhang, Q.; Ni, W.; Liu, Y.; Li, Z.; He, G.; Li, C.; Kan, B.; Chen, Y. Solution-Processed and High-Performance Organic Solar Cells Using Small Molecules with a Benzodithiophene Unit. *J. Am. Chem. Soc.* **2013**, *135*, 8484−8487.
(7) Wallquist, O.; Lenz, R. 20 Years of DPP Pigments − Future Perspectives. *Macromol. Symp.* **2002**, *187*, 617−630.
(8) Qu, S.; Tian, H. Diketopyrrolopyrrole (DPP)-based Materials for Organic Photovoltaics. *Chem. Commun.* **2012**, *48*, 3039−3051.
(9) Nielsen, C. B.; Turbiez, M.; McCulloch, I. Recent Advances in the Development of Semiconducting DPP-Containing Polymers for Transistor Applications. *Adv. Mater.* **2013**, *25*, 1859−1880.
(10) Biniek, L.; Schroeder, B. C.; Nielsen, C. B.; McCulloch, I. Recent Advances in High Mobility Donor−acceptor Semiconducting Polymers. *J. Mater. Chem.* **2012**, *22*, 14803−14813.
(11) Tamayo, A. B.; Walker, B.; Nguyen, T.-Q. A Low Band Gap, Solution Processable Oligothiophene with a Diketopyrrolopyrrole Core for Use in Organic Solar Cells. *J. Phys. Chem. C* **2008**, *112*, 11545−11551.
(12) Walker, B.; Tamayo, A. B.; Dang, X. D.; Zalar, P.; Seo, J. H.; Garcia, A.; Tantiwiwat, M.; Nguyen, T. Q. Nanoscale Phase Separation and High Photovoltaic Efficiency in Solution-Processed, Small-Molecule Bulk Heterojunction Solar Cells. *Adv. Funct. Mater.* **2009**, *19*, 3063−3069.
(13) Loser, S.; Bruns, C. J.; Miyauchi, H.; Ortiz, R. P.; Facchetti, A.; Stupp, S. I.; Marks, T. J. A Naphthodithiophene-Diketopyrrolopyrrole Donor Molecule for Efficient Solution-Processed Solar Cells. *J. Am. Chem. Soc.* **2011**, *133*, 8142−8145.
(14) Huang, J.; Zhan, C.; Zhang, X.; Zhao, Y.; Lu, Z.; Jia, H.; Jiang, B.; Ye, J.; Zhang, S.; Tang, A.; Liu, Y.; Pei, Q.; Yao, J. Solution-Processed DPP-Based Small Molecule that Gives High Photovoltaic Efficiency with Judicious Device Optimization. *ACS Appl. Mater. Interfaces* **2013**, *5*, 2033−2039.
(15) Pan, J.; Zuo, L.; Hu, X.; Fu, W.; Chen, M.; Fu, L.; Gu, X.; Shi, H.; Shi, M.; Li, H.; Chen, H.-Z. Star-Shaped D−A Small Molecules Based on Diketopyrrolopyrrole and Triphenylamine for Efficient Solution-Processed Organic Solar Cells. *ACS Appl. Mater. Interfaces* **2013**, *5*, 972−980.
(16) Chen, M.; Fu, W.; Shi, M.; Hu, X.; Pan, J.; Ling, J.; Li, H.; Chen, H.-Z. An Ester-Functionalized Diketopyrrolopyrrole Molecule with Appropriate Energy Levels for Application in Solution-processed Organic Solar Cells. *J. Mater. Chem. A* **2013**, *1*, 105−111.
(17) Liu, J.; Walker, B.; Tamayo, A.; Zhang, Y.; Nguyen, T.-Q. Effects of Heteroatom Substitutions on the Crystal Structure, Film Formation, and Optoelectronic Properties of Diketopyrrolopyrrole-Based Materials. *Adv. Funct. Mater.* **2013**, *23*, 47−56.
(18) Sonar, P.; Ng, G.-M.; Lin, T.-T.; Dodabalapur, A.; Chen, Z.-K. Solution Processable Low Bandgap Diketopyrrolopyrrole (DPP) based Derivatives: Novel Acceptors for Organic Solar Cells. *J. Mater. Chem.* **2010**, *20*, 3626−3636.
(19) Walker, B.; Liu, J.; Kim, C.; Welch, G. C.; Park, J. K.; Lin, J.; Zalar, P.; Proctor, C. M.; Seo, J. H.; Bazan, G. C.; Nguyen, T.-Q. Optimization of Energy Levels by Molecular Design: Evaluation of Bis-diketopyrrolopyrrole Molecular Donor Materials for Bulk Heterojunction Solar Cells. *Energy Environ. Sci.* **2013**, *6*, 952−962.
(20) Lin, Y.; Cheng, P.; Li, Y.; Zhan, X. A 3D Star-shaped Non-fullerene Acceptor for Solution-Processed Organic Solar Cells with a High Open-circuit Voltage of 1.18 V. *Chem. Commun.* **2012**, *48*, 4773−4775.
(21) Lee, O.- P.; Yiu, A.-T.; Beaujuge, P.-M.; Woo, C.-H.; Holcombe, T.-W.; Millstone, J.-E.; Douglas, J.-D.; Chen, M.-S.; Fréchet, J. M. J. Efficient Small Molecule Bulk Heterojunction Solar Cells with High Fill Factors via Pyrene-Directed Molecular Self-Assembly. *Adv. Mater.* **2011**, *23*, 5359−5363.
(22) Liu, J.; Sun, Y.; Moonsin, P.; Kuik, M.; Proctor, C. M.; Lin, J.; Hsu, B. B.; Promarak, V.; Heeger, A. J.; Nguyen, T. Q. *Tri*-Diketopyrrolopyrrole Molecular Donor Materials for High-Performance Solution-Processed Bulk Heterojunction Solar Cells. *Adv. Mater.* **2013**, *25*, 5898−5903.
(23) Choi, Y. S.; Jo, W. H. A Strategy to Enhance Both V_{OC} and J_{SC} of A−D−A Type Small Molecules based on Diketopyrrolopyrrole for High Efficient Organic Solar Cells. *Org. Electron.* **2013**, *14*, 1621−1628.
(24) Lin, Y.; Dam, H. F.; Andersen, T. R.; Bundgaard, E.; Fu, W.; Chen, H.; Krebs, F. C.; Zhan, X. Ambient Roll-to-roll Fabrication of Flexible Solar Cells Based on Small Molecules. *J. Mater. Chem. C* **2013**, *1*, 8007−8010.
(25) Bai, H.; Cheng, P.; Wang, Y.; Ma, L.; Li, Y.; Zhu, D.; Zhan, X. A Bipolar Small Molecule based on Indacenodithiophene and Diketopyrrolopyrrole for Solution Processed Organic Solar Cells. *J. Mater. Chem. A* **2014**, *2*, 778−784.
(26) Zhang, Y.; Liu, J.; Nguyen, T.-Q. Photoresponse of Donor/Acceptor Blends in Organic Transistors: A Tool for Understanding Field-Assisted Charge Separation in Small Molecule Bulk Heterojunction Solar Cells. *ACS Appl. Mater. Interfaces* **2013**, *5*, 2347−2353.
(27) Mazzio, K. A.; Yuan, M.; Okamoto, K.; Luscombe, C. K. Oligoselenophene Derivatives Functionalized with a Diketopyrrolopyrrole Core for Molecular Bulk Heterojunction Solar Cells. *ACS Appl. Mater. Interfaces* **2011**, *3*, 271−278.
(28) Lin, Y.; Ma, L.; Li, Y.; Liu, Y.; Zhu, D.; Zhan, X. A Solution-Processable Small Molecule Based on Benzodithiophene and Diketopyrrolopyrrole for High-Performance Organic Solar Cells. *Adv. Energy Mater.* **2013**, *3*, 1166−1170.
(29) Lin, Y.; Li, Y.; Zhan, X. A Solution-Processable Electron Acceptor Based on Dibenzosilole and Diketopyrrolopyrrole for Organic Solar Cells. *Adv. Energy Mater.* **2013**, *3*, 724−728.
(30) Huang, J.; Wang, X.; Zhang, X.; Niu, Z.; Lu, Z.; Jiang, B.; Sun, Y.; Zhan, C.; Yao, J. Additive-Assisted Control over Phase-Separated Nanostructures by Manipulating Alkylthienyl Position at Donor Backbone for Solution-Processed, Non-Fullerene, All-Small-Molecule Solar Cells. *ACS Appl. Mater. Interfaces* **2014**, *6*, 3853−3862.
(31) Chen, T. L.; Zhang, Y.; Smith, P.; Tamayo, A.; Liu, Y.; Ma, B. Diketopyrrolopyrrole-Containing Oligothiophene-Fullerene Triads and Their Use in Organic Solar Cells. *ACS Appl. Mater. Interfaces* **2011**, *3*, 2275−2280.
(32) Qiao, Y.; Guo, Y.; Yu, C.; Zhang, F.; Xu, W.; Liu, Y.; Zhu, D. Diketopyrrolopyrrole-Containing Quinoidal Small Molecules for High-Performance, Air-Stable, and Solution-Processable n-Channel Organic Field-Effect Transistors. *J. Am. Chem. Soc.* **2012**, *134*, 4084−4087.
(33) Zhong, H.; Smith, J.; Rossbauer, S.; White, A. J. P.; Anthopoulos, T. D.; Heeney, M. Air-Stable and High-Mobility n-Channel Organic Transistors Based on Small-Molecule/Polymer Semiconducting Blends. *Adv. Mater.* **2012**, *24*, 3205−3211.

(34) Palai, A. K.; Lee, J.; Das, S.; Lee, J.; Cho, H.; Park, S.-U.; Pyo, S. A Diketopyrrolopyrrole Containing Molecular Semiconductor: Synthesis, Characterization and Solution-processed 1D-Microwire based Electronic Devices. *Org. Electron.* **2012**, *13*, 2553−2560.
(35) Suraru, S.-L.; Zschieschang, U.; Klauk, H.; Würthner, F. Diketopyrrolopyrrole as a p-Channel Organic Semiconductor for High Performance OTFTs. *Chem. Commun.* **2011**, *47*, 1767−1769.
(36) Qu, S.; Wu, W.; Hua, J.; Kong, C.; Long, Y.; Tian, H. New Diketopyrrolopyrrole (DPP) Dyes for Efficient Dye-Sensitized Solar Cells. *J. Phys. Chem. C* **2010**, *114*, 1343−1349.
(37) Qu, S.; Qin, C.; Islam, A.; Wu, Y.; Zhu, W.; Hua, J.; Tian, H.; Han, L. A Novel D-A-π-A Organic Sensitizer Containing a Diketopyrrolopyrrole Unit with a Branched Alkylchain for Highly Efficient and Stable Dye-sensitized Solar Cells. *Chem. Commun.* **2012**, *48*, 6972−6974.
(38) Favereau, L.; Warnan, J.; Anne, F. B.; Pellegrin, Y.; Blart, E.; Jacquemin, D.; Odobel, F. Diketopyrrolopyrrole-zinc Porphyrin, a Tuned Panchromatic Association for Dye-sensitized Solar Cells. *J. Mater. Chem. A* **2013**, *1*, 7572−7575.
(39) Qu, Y.; Hua, J.; Tian, H. Colorimetric and Ratiometric Red Fluorescent Chemosensor for Fluoride Ion Based on Diketopyrrolopyrrole. *Org. Lett.* **2010**, *12*, 3320−3323.
(40) Deng, L.; Wu, W.; Guo, H.; Zhao, J.; Ji, S.; Zhang, X.; Yuan, X.; Zhang, C. Colorimetric and Ratiometric Fluorescent Chemosensor Based on Diketopyrrolopyrrole (DPP) for Selective Detection of Thiols: An Experimental and Theoretical Study. *J. Org. Chem.* **2011**, *76*, 9294−9304.
(41) Schutting, S.; Borisov, S. M.; Klimant, I. Diketo-Pyrrolo-Pyrrole Dyes as New Colorimetric and Fluorescent pH Indicators for Optical Carbon Dioxide Sensors. *Anal. Chem.* **2013**, *85*, 3271−3279.
(42) Lin, Y.; Zhang, Z.-G.; Li, Y.; Zhu, D.; Zhan, X. One, Two and Three-Branched Triphenylamine−Oligothiophene Hybrids for Solution-Processed Solar Cells. *J. Mater. Chem. A* **2013**, *1*, 5128−5135.
(43) Burckstummer, H.; Weissenstein, A.; Bialas, D.; Würthner, F. Synthesis and Characterization of Optical and Redox Properties of Bithiophene-Functionalized Diketopyrrolopyrrole Chromophores. *J. Org. Chem.* **2011**, *76*, 2426−2432.
(44) Facchetti, A.; Vaccaro, L.; Marrocchi, A. Semiconducting Polymers Prepared by Direct Arylation Polycondensation. *Angew. Chem., Int. Ed.* **2012**, *51*, 3520−3523.
(45) Mercier, L. G.; Leclerc, M. Direct (Hetero) Arylation: A New Tool for Polymer Chemists. *Acc. Chem. Res.* **2013**, *46*, 1597−1605.
(46) Okamoto, K.; Zhang, J.; Housekeeper, J. B.; Marder, S. R.; Luscombe, C. K. C−H Arylation Reaction: Atom Efficient and Greener Syntheses of π-Conjugated Small Molecules and Macromolecules for Organic Electronic Materials. *Macromolecules* **2013**, *46*, 8059−8078.
(47) Tan, Y.; Hartwig, J. F. Assessment of the Intermediacy of Arylpalladium Carboxylate Complexes in the Direct Arylation of Benzene: Evidence for C−H Bond Cleavage by "Ligandless" Species. *J. Am. Chem. Soc.* **2011**, *133*, 3308−3311.
(48) Wakioka, M.; Nakamura, Y.; Hihara, Y.; Ozawa, F.; Sakaki, S. Factors Controlling the Reactivity of Heteroarenes in Direct Arylation with Arylpalladium Acetate Complexes. *Organometallics* **2013**, *32*, 4423−4430.
(49) Caron, L.; Campeau, L.-C.; Fagnou, K. Palladium-Catalyzed Direct Arylation of Nitro-Substituted Aromatics with Aryl Halides. *Org. Lett.* **2008**, *10*, 4533−4536.
(50) Gorelsky, S. I.; Lapointe, D.; Fagnou, K. Analysis of the Palladium-Catalyzed (Aromatic) C-H Bond Metalation−Deprotonation Mechanism Spanning the Entire Spectrum of Arenes. *J. Org. Chem.* **2012**, *77*, 658−668.
(51) Schipper, D. J.; Fagnou, K. Direct Arylation as a Synthetic Tool for the Synthesis of Thiophene-Based Organic Electronic Materials. *Chem. Mater.* **2011**, *23*, 1594−1600.
(52) Liu, C.-Y.; Zhao, H.; Yu, H. Efficient Synthesis of 3,4-Ethylenedioxythiophene (EDOT)-Based Functional π-Conjugated Molecules through Direct C−H Bond Arylations. *Org. Lett.* **2011**, *13*, 4068−4071.
(53) Burke, D. J.; Lipomi, D. J. Green Chemistry for Organic Solar Cells. *Energy Environ. Sci.* **2013**, *6*, 2053−2066.
(54) Liu, S.-Y.; Li, H.-Y.; Shi, M.-M.; Jiang, H.; Hu, X.-L.; Li, W.-Q.; Fu, L.; Chen, H.-Z. Pd/C as a Clean and Effective Heterogeneous Catalyst for C−C Couplings toward Highly Pure Semiconducting Polymers. *Macromolecules* **2012**, *45*, 9004−9009.
(55) Liu, S.-Y.; Shi, M.; Huang, J.; Jin, Z.; Hu, X.; Pan, J.; Li, H.; Jen, A. K.-Y.; Chen, H.-Z. C−H Activation: Making Diketopyrrolopyrrole Derivatives Easily Accessible. *J. Mater. Chem. A* **2013**, *1*, 2795−2805.
(56) Zhang, J.; Kang, D.-Y.; Barlow, S.; Marder, S. R. Transition Metal-catalyzed C−H Activation as a Route to Structurally Diverse Di(arylthiophenyl)-diketopyrrolopyrroles. *J. Mater. Chem.* **2012**, *22*, 21392−21392.
(57) Guo, Q.; Dong, J.; Wan, D.; Wu, D.; You, J. Modular Establishment of a Diketopyrrolopyrrole -Based Polymer Library via Pd-Catalyzed Direct C−H (Hetero)arylation: a Highly Efficient Approach to Discover Low-Bandgap Polymers. *Macromol. Rapid Commun.* **2013**, *34*, 522−527.
(58) Liu, S.-Y.; Fu, W.-F.; Xu, J.-Q.; Fan, C.-C.; Jiang, H.; Shi, M.; Li, H.-Y.; Chen, J.-W.; Cao, Y.; Chen, H.-Z. A Direct Arylation-derived DPP-based Small Molecule for Solution-Processed Organic Solar Cells. *Nanotechnology* **2014**, *25*, 014006.
(59) Winnik, F. M. Photophysics of Preassociated Pyrenes in Aqueous Polymer Solutions and in other Organized Media. *Chem. Rev.* **1993**, *93*, 587−614.
(60) Figueira-Duarte, T. M.; Müllen, K. Pyrene-Based Materials for Organic Electronics. *Chem. Rev.* **2011**, *111*, 7260−7314.
(61) Feng, X.; Hu, J.-Y.; Iwanaga, F.; Seto, N.; Redshaw, C.; Elsegood, M. R. J.; Yamato, T. Blue-Emitting Butterfly-Shaped 1,3,5,9-Tetraarylpyrenes: Synthesis, Crystal Structures, and Photophysical Properties. *Org. Lett.* **2013**, *15*, 1318−1321.
(62) Moorthy, J. N.; Natarajan, P.; Venkatakrishnan, P.; Huang, D.-F.; Chow, T. J. Steric Inhibition of π-Stacking: 1,3,6,8-Tetraarylpyrenes as Efficient Blue Emitters in Organic Light Emitting Diodes (OLEDs). *Org. Lett.* **2007**, *9*, 5215−5218.
(63) Sonar, P.; Soh, M. S.; Cheng, Y. H.; Henssler, J. T.; Sellinger, A. 1,3,6,8-Tetrasubstituted Pyrenes: Solution-Processable Materials for Application in Organic Electronics. *Org. Lett.* **2010**, *12*, 3292−3295.
(64) Uchimura, M.; Watanabe, Y.; Araoka, F.; Watanabe, J.; Takezoe, H.; Konishi, G. Development of Laser Dyes to Realize Low Threshold in Dye-Doped Cholesteric Liquid Crystal Lasers. *Adv. Mater.* **2010**, *22*, 4473−4478.
(65) Xia, R.; Lai, W.-Y.; Levermore, P. A.; Huang, W.; Bradley, D. D. C. Low-Threshold Distributed-Feedback Lasers Based on Pyrene-Cored Starburst Molecules with 1,3,6,8-Attached Oligo(9,9-Dialkylfluorene) Arms. *Adv. Funct. Mater.* **2009**, *19*, 2844−2850.
(66) You, J.; Li, G.; Wang, R.; Nie, Q.; Wang, Z.; Li, J. Pyrene-cored Dendrimer with Carbazole Derivatives as Dendrons: Synthesis, Properties and Application in White Light-Emitting Diode. *Phys. Chem. Chem. Phys.* **2011**, *13*, 17825−17830.
(67) Zou, L.; Wang, X.-Y.; Shi, K.; Wang, J.-Y.; Pei, J. Fusion at the Non-K-Region of Pyrene: An Alternative Strategy to Extend the π-Conjugated Plane of Pyrene. *Org. Lett.* **2013**, *15*, 4378−4481.
(68) Bernhardt, S.; Kastler, M.; Enkelmann, V.; Baumgarten, M.; Müllen, K. Pyrene as Chromophore and Electrophore: Encapsulation in a Rigid Polyphenylene Shell. *Chem.—Eur. J.* **2006**, *12*, 6117−6128.
(69) Zhang, H.; Wang, Y.; Shao, K.; Liu, Y.; Chen, S.; Qiu, W.; Sun, X.; Qi, T.; Ma, Y.; Yu, G.; Su, Z.; Zhu, D. Novel Butterfly Pyrene-based Organic Semiconductors for Field Effect Transistors. *Chem. Commun.* **2006**, 755−757.
(70) Takemoto, K.; Karasawa, M.; Kimura, M. Solution-Processed Bulk-Heterojunction Solar Cells containing Self-Organized Disk-Shaped Donors. *ACS Appl. Mater. Interfaces* **2012**, *4*, 6289−6294.
(71) Kim, J.-H.; Kim, H. U.; Kang, I.-N.; Lee, S. K.; Moon, S.-J.; Shin, W. S.; Hwang, D.-H. Incorporation of Pyrene Units to Improve Hole Mobility in Conjugated Polymers for Organic Solar Cells. *Macromolecules* **2012**, *45*, 8628−8638.
(72) Frisch, M. J.; Trucks, G. W.; Schlegel, H. B.; Scuseria, G. E.; Robb, M. A.; Cheeseman, J. R.; Scalmani, G.; Barone,V.; Mennucci, B.;

Petersson, G. A.; Nakatsuji, H.; Caricato, M.; Li, X.; Hratchian, H. P.; Izmaylov, A. F.; Bloino, J.; Zheng, G.; Sonnenberg, J. L.; Hada, M.; Ehara,M.; Toyota, K.; Fukuda, R.; Hasegawa, J.; Ishida, M.; Nakajima, T.; Honda, Y.; Kitao, O.; Nakai, H.; Vreven, T.; Montgomery, J. A., Jr.; Peralta, J. E.; Ogliaro, F.; Bearpark, M.; Heyd, J. J.; Brothers, E.; Kudin, K. N.; Staroverov, V. N.; Kobayashi, R.; Normand, J.; Raghavachari, K.; Rendell, A.; Burant, J. C.; Iyengar, S. S.; Tomasi, J.; Cossi, M.; Rega, N.; Millam, J. M.; Klene, M.; Knox, J. E.; Cross, J. B.; Bakken, V.; Adamo, C.; Jaramillo, J.; Gomperts, R.; Stratmann, R. E.; Yazyev, O.; Austin, A. J.; Cammi, R.; Pomelli, C.; Ochterski, J. W.; Martin, R. L.; Morokuma, K.; Zakrzewski, V. G.; Voth, G. A.; Salvador, P.; Dannenberg, J. J.; Dapprich, S.; Daniels, A. D.; Farkas, O.; Foresman, J. B.; Ortiz, J. V.; Cioslowski, J.; Fox, D. J. *Gaussian09*; Gaussian, Inc.: Wallingford, CT, 2009.

(73) Becke, A. D. Density-functional Thermochemistry. III. The Role of Exact Exchange. *J. Chem. Phys.* **1993**, *98*, 5648−5652.